J Nanopart Res (2012) 14:1075
DOI 10.1007/s11051-012-1075-2

RESEARCH PAPER

Incorporating different vegetable oils into an aqueous dispersion of hybrid organic nanoparticles

Pieter Samyn · Gustaaf Schoukens · Dirk Stanssens · Leo Vonck · Henk Van den Abbeele

Received: 4 March 2012 / Accepted: 17 July 2012 / Published online: 1 August 2012

Abstract Different vegetable oils including soy oil, high-oleic sunflower oil, corn oil, castor oil (CO), rapeseed oil, and hydrogenated CO were added to the imidization reaction of poly(styrene–maleic anhydride) or SMA, with ammonium hydroxide in aqueous medium. The oils favorably reduce viscosity during ammonolysis of the anhydride moieties and increase the maximum solid content of the dispersed imidized SMA to at least 50 wt%, compared to a maximum of 35 wt% for pure imidized SMA. The viscosity of imidized SMA with polyunsaturated oils was generally larger than for monosaturated oils, but it was highest for COs due to high contents of hydroxyl groups. Depending on the oil reactivity, homogeneous or core–shell nanoparticles with 20–60 nm diameters formed. The interactions of oil and organic phase were studied by Fourier-transform infrared spectroscopy, indicating qualitative variances between different oils, the fraction imidized SMA and remaining fraction of ammonolyzed SMA without leakage of oil upon diluting the dispersion and precipitation at low pH. A quantitative analysis with calculation of imide contents, amounts of reacted oil and chemical interactions was made by Fourier-transform-Raman spectroscopy suggesting that most interactions take place around the unsaturated oil moieties and ammonolyzed anhydride.

Keywords Nanoparticles · Core–shell · Encapsulation · Copolymer · Vegetable oil

P. Samyn (✉)
Institute for Forest Utilization, Albert-Lüdwigs-University Freiburg, Werthmannstrasse 6, 79085 Freiburg, Germany
e-mail: Pieter.Samyn@fobawi.uni-freiburg.de

G. Schoukens
Department of Textiles, Ghent University, Technologiepark 907, 9052 Zwijnaarde, Belgium

D. Stanssens · L. Vonck · H. Van den Abbeele
Topchim N.V., Nijverheidstraat 98, 2160 Wommelgem, Belgium

Introduction

The encapsulation of hydrophobic ingredients provides good opportunities to create functional materials, with the core product protected and stabilized by a shell layer. Through controlled retention, delayed release or transport those compounds provide active properties. Such materials can be used as perfumes (Sansukcharearnpon et al. 2010), pharmaceuticals and cosmetics (Fairhurst and Loxley 2008) fabric treatment products (Zhong et al. 2005), fluorescent dyes (Mazur 2008), printing inks (Leelajariyakul et al. 2008), lubricants (Tian et al. 2007), heat regulating agents (Hawlader et al. 2003), or coating pigments (Nguyen et al. 2008) including rheology modifiers, optical brighteners, UV stabilizers, or even sophisticated microreactors (Lee et al. 2007). Before the

capsules are favorably applicable, they should be delivered in a suitable dispersant. However, organic solvents are often forbidden or should be limited due to process compatibility, safety, and environmental issues: e.g., material handling in the paper industry is based on aqueous suspensions of fibers and fillers (Mogridge et al. 2002), the performance of dyes depends on the pH of the dispersant (Horie et al. 2007), or cosmetic products should not irritate the skin (Yow et al. 2005). Therefore, the encapsulated products should preferentially be available in a stable and neutral waterborne dispersion. Moreover, the encapsulated products should mostly be insoluble in water after removal of dispersant to resist leaching and improve durability in the dried state. Non-water-soluble materials such as vegetable oils, paraffin oils, waxes, polyolefins, silicones, alkanes,… can be transformed into stable waterborne specimens through compatibilization with a surface agent in the capsule wall. In selecting a polymer for the capsule wall, the following design criteria must be considered: (i) easy synthesis allowing for high amount of encapsulated agent and high solid content, (ii) good mechanical and thermal stability, and (iii) avoiding additional surfactants for stabilizing the dispersion, which may often interfere with the polycondensation reaction (Mizuno and Taguchi 2005) or have negative effects on the properties of dried capsules such as decreased cohesiveness of the wall, or reduce adhesiveness when applied to a product or substrate.

At the microscale, supporting materials for microcapsules of paraffin include HDPE (Hong and Xin-shi 2000; Inaba and Tu 1997; Liu et al. 2006a), styrene [St]–butadiene–St copolymers (Xiao et al. 2002), bisphenol-A epoxy or St–ethylene–butylene–St copolymers (Peng et al. 2004), and polyethylene glycol/acrylic blends (Alkan et al. 2006). Other resins such as polyurethane, melamine-formaldehyde, urea-formaldehyde were used for encapsulation of *n*-octadecane (Kim and Kim 2005; Su et al. 2006), or alkanes (Zhang et al. 2005). However, some of them cause health problems and are synthesized in an intermediate solvent phase. Bio-based shell materials were consequently developed, such as ethylcellulose microcapsules in combination with rosemary oil by the phase separation method (Voncina et al. 2009), or chitosan for encapsulation of fish oil and citronella oil (Klaypradit and Huang 2008; Hsieh et al. 2006), alginates were used for sunflower oil (Abang et al. 2012), porous starch microspheres for plant oils (Glenn et al. 2010), and β-cyclodextrin for cinnamon oil (Petrovic et al. 2010). However, they often present lower thermal stability. The most direct method for formation of the capsules includes interfacial polycondensation reactions (Frere et al. 1998), in a mini-emulsion system (Torini et al. 2005). Other techniques employ oil encapsulation by powder spray drying and fluidized bed agglomeration (Jafari et al. 2008a; Turchiuli et al. 2005) with different efficiency (Fuchs et al. 2006). This technique was especially used for encapsulating olive oil with different shells (Calvo et al. 2010), rapeseed oils (KOs, Domian and Wqsak 2008), and general oil/matrix/water systems (Adamiec and Marciniak 2004). More sophisticated techniques are based on precipitation in supercritical fluids (Martin et al. 2010). As our goal relies in the design of new functional materials for coating applications, a broader review on encapsulation of vegetable oils for food applications (Zuidam and Nedovic 2010) is beyond scope. As alternative shell materials, poly(St–maleic anhydride) or SMA may be beneficially used due to their functionality and chemical reactivity: it has a carboxyl and ether oxygen that can interact with functional fatty acid groups: Sari et al. (2008) prepared SMA/fatty acid composites as stable phase change materials, or Shulkin and Stöver (2002) made microcapsules of acetate or dodecanol by interfacial polyaddition of SMA with amines, Su et al. (2007) formed microcapsules with octadecane and hydrolyzed SMA as a surfactant, and Rong et al. (2004) made gelatin/SMA microcapsules by complex coacervation.

At the nanoscale, the synthesis of functional nanocapsules has become a more emerging research field, and possibilities for encapsulating vegetable oils at this level have been more recently explored. Nanocapsules of fish oil could be made by controlled spray drying (Jafari et al. 2008b), or oil core nanoparticles could be obtained with a silica shell (Jovanovic et al. 2005). However, most methods are based on chemical reactions to form a polymer shell (Luo and Gu 2006), as e.g., hydrophobic compounds were nanoencapsulated by a one-step mini-emulsion polymerization (Luo and Zhou 2004). The high specific surface area and favorable presentation of reactive groups in nanospheres make them good candidates for active capsules, while the controlled orientation of molecular groups at the nanoscale may additionally contribute to better assembly and higher specificity:

the self-organization of molecular structures often spontaneously forms micelles or liposomes. Classical methods for nanoencapsulation include direct phase separation in mini-emulsion polymerization (Landfester 2009), formation of micelles by block copolymer assembly (Kim and Tation 2007), layer-by-layer adsorption of polyelectrolytes on liquid cores with specific surfactants (Szczepanowicz et al. 2010) polymer brush grafting from nanoparticles with cross-linking (Mu et al. 2009), or dendrimer synthesis (Esumi 2003). Bae et al. (2007) synthesized oil-encapsulating PEO–PPO–PEO/PEG nanocapsules by dissolving oil and the amine-reactive block copolymer in dichloromethane and subsequently dispersing it an aqueous solution by aid of ultrasonication. The latter techniques allow for good control over size and shape of the core–shell structure, but involve rather complex synthesis and are less suited for industrial production.

The simplest method comprises direct encapsulation of liquids by phase separation during polymerization. However, it is often more difficult in achieving a stable and integrated morphology with a well-controlled nanostructure. Therefore, mini-emulsion polymerization of nanocapsules induced by self-organization was developed using reversible addition fragmentation transfer of hydrolyzed SMA (Luo and Gu 2007). It is known that SMA forms different nanoscale structures and can be applied as a template for nanoscale materials (Malardier-Jugroot et al. 2005). In the presence of oils, the hydrolyzed SMA may form micelles due to local orientation of copolymer fragments depending on the stiffness of the polymer chain (Tao et al. 2008). In parallel, it may simultaneously play the role of surfactant and contribute to stability of hydrophobic encapsulant (Braun et al. 2001). At present, however, the thermomechanical weakness of such SMA polymer shell can be an obstruction for retaining hydrophobic agents during further processing (drying and pressing operations), depending on the nanometer shell thickness and relatively low glass transition temperature. Therefore, encapsulation and thermal stabilization of the organic phase by chemical conversion could be simultaneously controlled by self-assembly of the organic and oil phase in combination with subsequent imidization of the anhydride moieties into a more stable shell. We previously demonstrated that the imidization of SMA leads to an aqueous nanoparticle dispersion with better thermal stability (Samyn et al. 2012a). In this research, we further present the formation of nanometer capsules by imidization of SMA in the presence of vegetable oil.

Experiments

Materials

A copolymer of SMA, with molecular weight $M_w = 80{,}000$ g mol^{-1} and a ratio of 26 mol% maleic anhydride (MA) to 74 mol% St, was provided by Polyscope (Geleen, The Netherlands) as pellets and used as such. Ammonium hydroxide was obtained from Belgocare (Niel, Belgium) as a 25 % aqueous solution (0.9 g/ml).

Different refined vegetable oils, including soy oil (SO), high-oleic sunflower oil (ZO), corn oil (MO), castor oil (CO), KO, and a hydrogenated CO (HCO) were used as received from Cargill Agricola S/A (Mairinque, SP, Brazil). The oil compositions and physical properties were extensively characterized in previous reports, using mid-infrared or Raman spectroscopy (Samyn et al. 2012b), and thermal analysis (Samyn et al. 2012c). Some physical oil properties are given in Table 1, including iodine value (IV), viscosity, and portions of saturated (%*S*), mono-unsaturated (%*M*) and poly-unsaturated (%*P*) fatty acids.

Synthesis

Hybrid organic nanoparticles were synthesized in a lab-scale autoclave with a volume of 1 l. The SMA was loaded together with a selected vegetable oil, ammonium hydroxide, and water. The weight ratio of oil to copolymer was 1:1 and the ratio of ammonium hydroxide to MA was 1:1.01. For a typical run, about 212 g SMA were loaded with 212 g oil, 38.7 g NH_4OH (25 %), and 380 g water. The temperature of the reaction mixture was stepwise increased to 160 °C at a constant rotation speed of 300 rpm. After an initial temperature rise to approximately 90 °C at a pressure of 1 bar, the reaction mixture was heated to the final reaction temperature with an increase in reaction pressure to 6 bar. The temperature and pressure profiles were recorded together with the electric power P to drive the anchor stirrer at given constant speed of 400 rpm. The power $P = \tau \times 2\pi r$ (torque τ and angular velocity $\omega = 2\pi r$) is a measure

Table 1 Characteristics of vegetable oils

Oil type	IV [g (I_2)/100 g oil]	Composition			Viscosity (cp)	Acid value	Peroxide value (meq/kg)	Saponification value [mg (KOH)/1 g oil]
		% *M*	% *P*	% *S*				
SO	122	25	61	14	69.3	<1	2.7	195
MO	112	28	58	14	64.2	<0.6	3.0	190
KO	101	61	25	14	72.3	<2	1.0	170
ZO	82	78	2	20	92.6	<0.6	4.8	180
CO	92	87	11	2	620	<2	1.2	183
HCO	<20	14	5	81	Wax	<1	1.0	165

for the change in viscosity of the reaction mixture. After 4 h, the reaction mixture was cooled to room temperature and evacuated from the reactor for further analysis.

In a reference experiment, 212 g SMA was imidized without oil under the same conditions as above. After cooling the reaction mixture, it was subsequently mixed with pure MO in a weight ratio of 1:1 to obtain the so-called "physically mixture" of imidized SMA and oil. The physically mixed dispersion was created while magnetically stirring for about 1 h at 30 °C. The pure imidized SMA and physical mixture with MO were further analyzed for comparison with the chemically modified materials.

Characterization

The SMA imidized in the presence of vegetable oils (chemical mixture), or after reaction under pure conditions and subsequent oil addition (physical mixture), were evaluated. The waterborne dispersions were characterized by pH-measurements (Knick 752 Cl, nr. 051489), solid content determination or SC (Mettler LP16/PM600 infrared drying and weighing), dynamic light scattering or DLS (Zetasizer Nano ZS, Malvern) and viscosity measurements (Brookfield, DV-II Pro). The polymer/oil substance was recovered from aqueous dispersions by water evaporation in a hot-air oven for 6 h at 100 °C and further drying under atmospheric conditions for 1 week. The materials were alternatively recovered from the aqueous dispersion by precipitation in acid environment (1 M sodium acetate/acetic acid buffer pH = 4), followed by filtration and drying in a hot-air oven for 6 h at 100 °C. A film of nanoparticle dispersions was deposited onto aluminum foil by bar-coating. The films were dried for 2 min in a hot-air oven (110 °C) and homogenized for at least 1 day under room conditions, before evaluation with optical microscopy (Olympus BX 51).

For transmission electron microscopy (TEM), the dispersions were diluted 100 times. The nanoparticles were adsorbed on a carbon grid and air-dried for evaluation on a Leo 912 Omega (Zeiss) microscope. Fourier-transform infrared spectroscopy (FTIR) was done in attenuated total reflection (ATR) mode in the spectral range of 4,000–650 cm^{-1} with a resolution of 4 cm^{-1} on a Perkin Elmer Spectrum 65 instrument: a 0.1 ml droplet of aqueous dispersion was placed onto the diamond crystal and diluted by stepwise adding water droplets of 0.1 ml up to a maximum of ten. The dried powders were further evaluated by incorporating them in a KBr pellet and measured against a background. The spectra were collected with a He–Ne light source between 4,000 and 400 cm^{-1} and a resolution of 4 cm^{-1}, averaged over 32 scans. Fourier-transform Raman (FT-Raman) spectra were collected on a Perkin Elmer Spectrum GX equipment, using a Nd:YAG laser power of 500 mW at a 4 cm^{-1} resolution and averaged over 64 scans. The dispersions were measured through a standard glass vial for liquids, and the dried powders were filled in a suited sample holder.

Results and discussion

Synthesis of hybrid organic nanoparticles

A preliminary study on the influence of copolymer precursor indicates that low-molecular SMA did not result in the formation of organic nanoparticles. The

intrinsic structure of high-molecular weight SMA seems more favorable for the formation of nanostructures (Malardier-Jugroot et al. 2005), most likely through the distribution of St and MA moieties and possibilities for self-organization. We selected a grade with 26 mol% MA due to ease of imidization (Samyn et al. 2012a). The reaction profiles and electrical power P for synthesis pure imidized SMA or hybrid imidized SMA/oil, are illustrated in Fig. 1.

- For a reactor loading of 212 g pure SMA, the power P constantly increases and saturates at an extremely high level exceeding the stirring capacity. The reaction did not favorably terminate and resulted in the formation of a viscous mixture. In this case, the aqueous dispersion of pure imidized SMA had SC = 50 wt%, and the phase separation indicated dispersion instabilities. The loading of pure SMA was subsequently reduced to 150 g, in parallel with lower power P as the viscosity of the reaction mixture decreased. The rise in viscosity with reaction time represents systematic ammonolysis of the SMA with ammonium hydroxide (Moore and Pickelman 1986). After 3 h, a drop in viscosity represents the start of imidization by ring-closing of ammonolyzed SMA. This viscosity profile proves successful formation of well-dispersed imidized nanoparticles, which are non-water soluble and separate from the homogeneous solution phase (Liu et al. 2006b). From these reaction profiles, the imidized SMA in aqueous dispersion have a maximum SC = 35 wt%.
- For a reactor loading of 212 g SMA and 212 g vegetable oil, the increase in power P delays in the presence of oil. This phenomenon may point to physical or chemical alterations in the reaction mixture. From physical perspective, the original water/oil reaction mixture is inhomogeneous and the creation of finely dispersed oil droplets under mechanical shear needs some time. The oil may act as a lubricant in this process and reduce the energy dissipation to create the oil/water interface. From chemical perspective, the ammonolysis of SMA and related increase in viscosity may be retarded by non-specific and preferential interaction between the ammonium hydroxide and oil. Otherwise, ammonolyzed SMA may directly react with the oil without inducing charge-related carboxylic interactions between ring-opened anhydride moieties. The maximum viscosity for aqueous SMA/oil reaction mixtures is lower than for pure SMA and the viscosity drop occurs after a shorter reaction time in the presence of oil (30–50 min earlier). This suggests that oil serves as a catalyst, and/or that the reaction is not proceeding as far as for pure imidized SMA. Indeed, later analysis confirms that the imide content for imidized SMA/oil is lower than for pure imidized SMA. In contrast to the synthesis of pure imidized SMA, particles did not precipitate onto the reactor wall and cleaning was done more easily. All imidization reactions of SMA/oil fluently terminated at SC = 50 wt%. The lower viscosity for synthesis of imidized SMA/oil beneficially lowers the energy consumption for stirring. This effect depends on the oil type and its reactivity, where CO causes highest viscosity, while poly-unsaturated oils (SO, MO) cause somewhat higher viscosity than mono-unsaturated oils (KO).

Physical characterization of hybrid organic nanoparticle dispersions

The aqueous dispersions of pure imidized SMA and imidized SMA/oil nanoparticles were homogeneous and stable in time without separation between oil, organic, and water phases. The physical characteristics of the nanoparticle dispersions are summarized in Table 2. The pH-value of pure imidized SMA nanoparticle dispersions is almost neutral (pH = 6.5–7), as the ammonolyzed (ring-opened) anhydride moieties have imidized to a far extent. The pH-value (pH = 5–6) of imidized SMA/oil nanoparticle dispersions is lower, as some carboxyl acid moieties remain as a result of ring-opened cyclic anhydrides. The experimental values of SC = 49–50 wt% agree with theoretical expectations from the respective reactor loadings, indicating that all materials favorably reacted. The high SC for imidized SMA/oil nanoparticle dispersions, is a clear advantage over pure imidized SMA. The viscosity of imidized SMA/oil dispersions (91–146 cp) is mostly lower than the pure imidized SMA (179 cp), except for reactions with CO (230 cp). It is not surprising that CO provides highest viscosity (see also Fig. 1c), due to the presence of hydroxyl groups in ricinoleic fatty acids that build hydrogen bonds throughout the dispersion. These

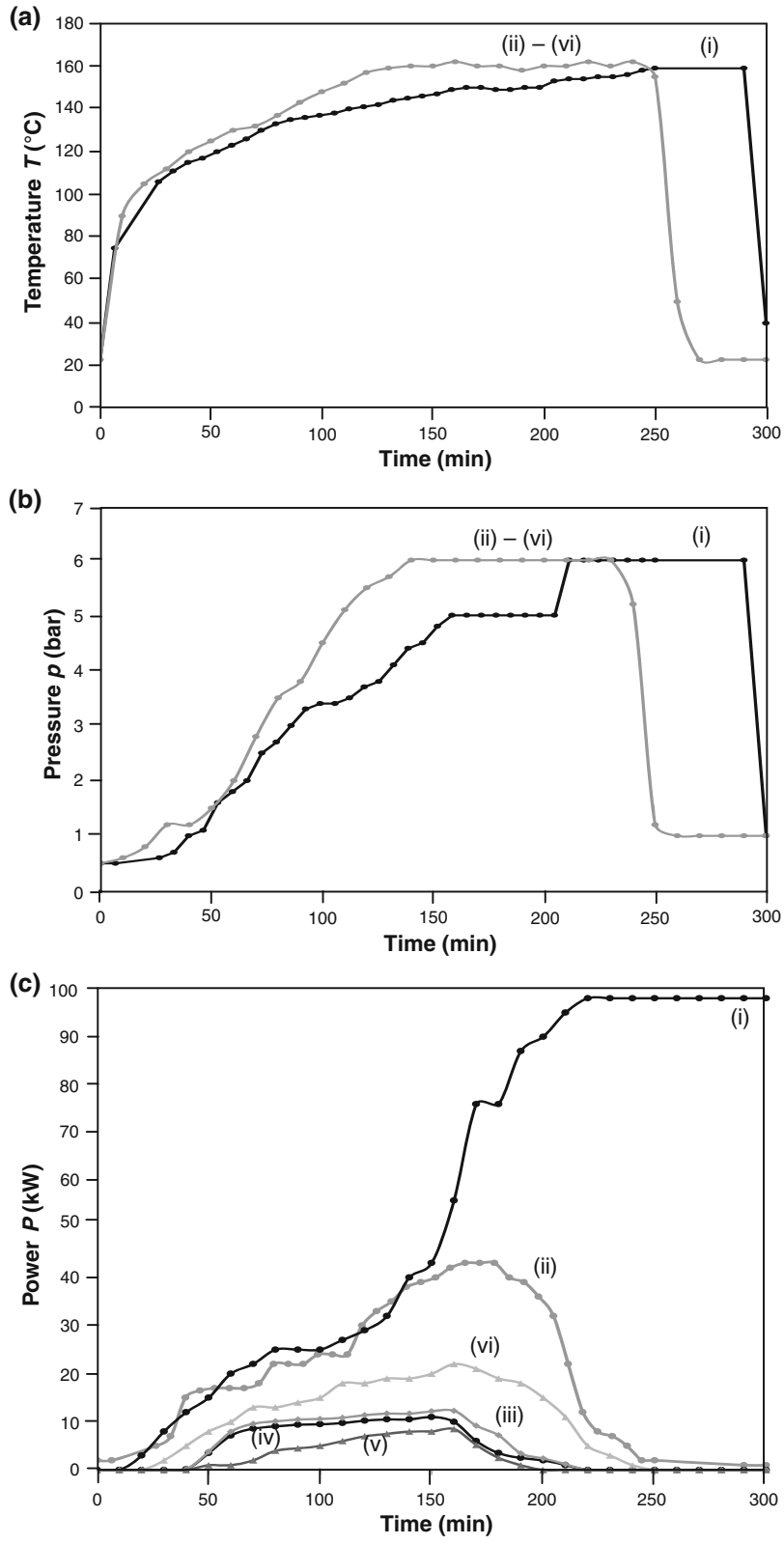

Fig. 1 Reaction profiles for hybrid organic nanoparticles: **a** temperature profile, **b** pressure profile, **c** electrical power, for following compositions: (*i*) pure imidized SMA, SC = 50 wt%, (*ii*) pure imidized SMA, SC = 35 wt%, (*iii*) imidized SMA/SO, SC = 50 wt%, (*iv*) imidized SMA/MO, SC = 50 wt%, (*v*) imidized SMA/KO, SC = 50 wt%, (*vi*) imidized SMA/CO, SC = 50 wt%

Table 2 Characteristics of hybrid organic nanoparticle dispersions containing imidized SMA/oil

Nanoparticle type	Ratio	pH	Solid content (%)	Viscosity (cp)	Nanoparticle size (DLS)	
					z-Average diameter (SD) (nm)	Polydispersity Δ (SD)
Imidized SMA	100/0	6.82	34.9	176	85 (0.15)	0.110 (0.02)
Imidized SMA/SO	50/50	5.48	49.8	146	149 (0.20)	0.163 (0.02)
Imidized SMA/MO	50/50	5.44	49.9	102	143 (0.18)	0.161 (0.02)
Imidized SMA/KO	50/50	5.43	49.5	91	156 (0.22)	0.137 (0.04)
Imidized SMA/ZO	50/50	5.38	48.8	134	143 (0.25)	0.176 (0.03)
Imidized SMA/CO	50/50	5.72	49.9	230	148 (0.55)	0.137 (0.07)
Imidized SMA/HCO	50/50	5.54	49.3	116	132 (0.60)	0.127 (0.07)

SD standard deviation

effects obviously diminish for reactions with hydrogenated oil (HCO). The viscosities of the imidized SMA/oil nanoparticle dispersions are somewhat higher than pure oils, but do not directly relate to the original oil viscosity (Table 1): so, the oils are likely shielded with an organic phase and the interface properties of the oil/water phase are determined by imidized SMA. It is known that pure SMA acts as a dispersing agent (Martinez et al. 2005), and thus may stabilize the oil/water mixture. Also in present system, imidized SMA obviously acts as a stabilizer: it theoretically first orients at the oil/water interface (Rong et al. 2004) and the water-soluble anhydride moieties later imidize (partially) at the oil droplet interface. The ammonolysis of SMA causes a ring-opening of the anhydride moieties, with consequently an increase in viscosity due to mutual interactions between COO^- and NH_3^+ moieties. However, the availability of ammonium hydroxide for ammonolysis may be limited through partial consumption by the oil, geometrical constraints, or orientation and conformation effects of SMA at the oil/water interface. These may indeed lead to lower imide content for imidized SMA/oil, as further calculated. The particle sizes of dispersed pure imidized SMA nanoparticles (85 nm) are smaller than imidized SMA/oil nanoparticles (132–156 nm). Moreover, the measured values for all hybrid nanoparticles are in a similar range and likely influenced by swelling and/or formation of an electrical double layer. The interlayer thickness and the presence of charged moieties is likely influenced by the acid pH-value of the dispersions. The charges in this layer contribute to the good dispersion stability and are confirmed by a Zeta-potential value of $\zeta = -60$ mV for pure imidized SMA or $\zeta = -40$ to -50 mV for imidized SMA/oil nanoparticles (at intrinsic pH of the dispersion). These values are within the range of ammonolyzed SMA solutions. By lowering the pH below 4, the Zeta-potential progressively increases within the range of $\zeta = 0$ to -20 mV with consequent colloidal instability and nanoparticle sedimentation.

The TEM images of pure imidized SMA and imidized SMA/oil nanoparticles are shown in Fig. 2. For pure imidized SMA, an average diameter of 80 nm is in relatively good agreement with DLS. For imidized SMA/oil, sizes and morphologies are more heterogeneous and depend on the oil type with average diameters of 20–60 nm for SO, MO, KO, ZO and 150–200 nm for CO and HCO. The latter show larger differences between TEM and DLS size measurements: the nanoparticles have a weak structure and are more prone to swelling, or the oils in dispersed state cause a "drag" on the nanoparticle interface and artificially increase the diameter by physical adsorption in aqueous conditions. The dimensional changes under drying are the first indication that the hybrid nanoparticles have a "dynamic" structure, where the oil phase has certain mobility respective to the organic phase. In ongoing studies, this effect can be more intensively characterized in parallel with possible effects of thermal oil release. The greyscale contrast in TEM indicates different material densities and suggests following morphologies:

- The SO and MO hybrid nanoparticles have a homogeneous shape with constant density of mixed oil and organic phase. Both SO and MO have high IV with mainly poly-unsaturated fatty acids that are very reactive at the C=C double

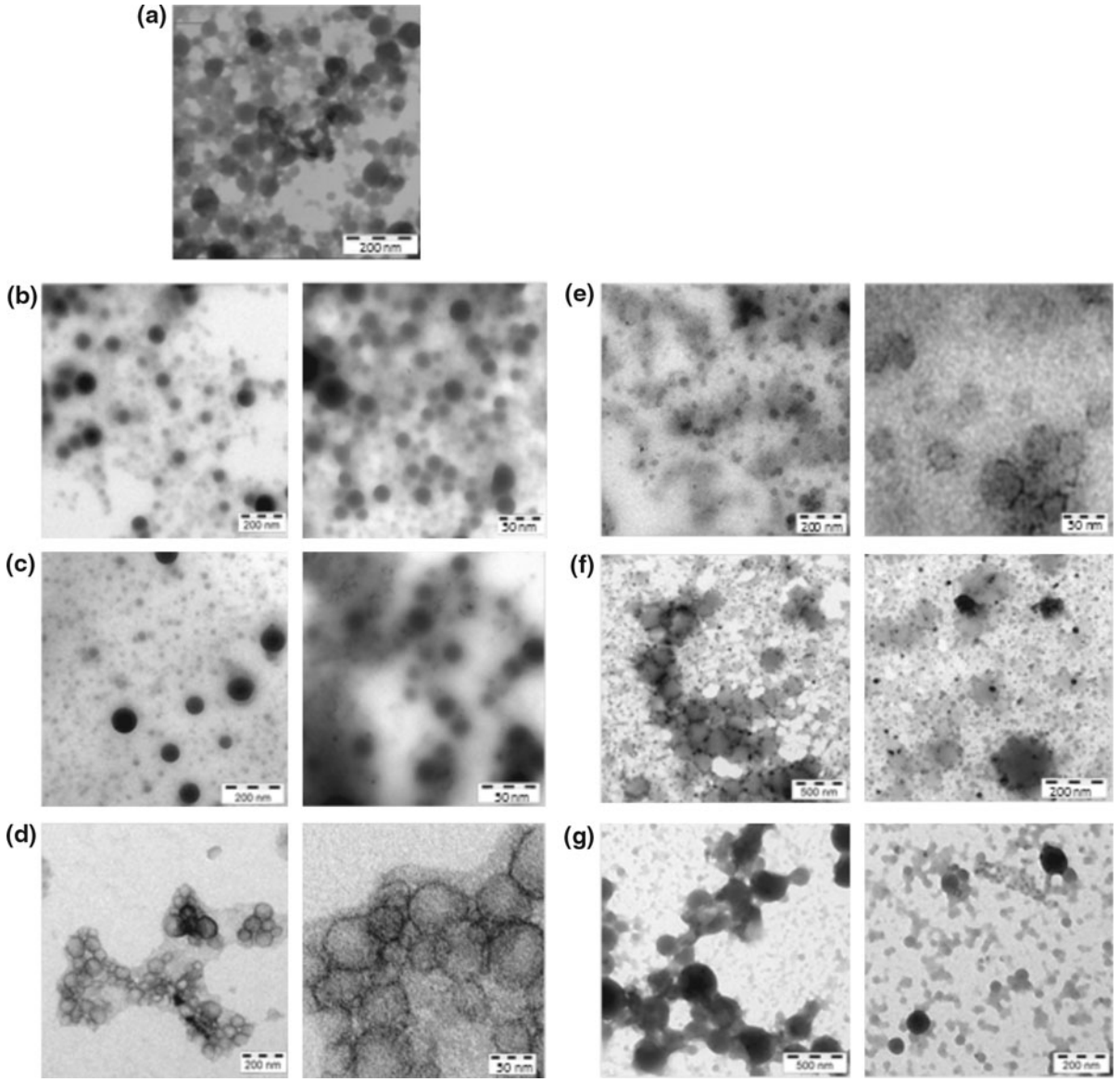

Fig. 2 TEM of hybrid organic nanoparticles including different vegetable oils, **a** pure imidized SMA, **b** imidized SMA/SO, **c** imidized SMA/MO, **d** imidized SMA/KO, **e** imidized SMA/ZO, **f** imidized SMA/CO, and **g** imidized SMA/HCO

bonds. Theoretically, a high density of C=C sites creates reactive places for interaction with the organic SMA phase. Therefore, it can be expected that both phases are well interconnected and form homogeneous nanoparticles.

- The ZO and KO hybrid nanoparticles have a dense border and rather form core–shell structures with a shell of 5–7 nm, and internal core of 30–40 nm in average. As this structure is weaker than bulk polymer nanoparticles of pure imidized SMA, different swelling properties were observed in DLS measurements. Both ZO and KO have intermediate IV with more mono-unsaturated fatty acids that are somewhat less reactive than poly-unsaturated ones. Thus, the possibilities for chemical interactions between oil and organic phases are theoretically lower and mainly happen at the water/oil interface to form the shell.
- The CO and HCO hybrid nanoparticles have larger diameters in agreement with previous DLS

measurements. For HCO, some large spherical caps measure up to 500 nm and may eventually be attributed to free oil droplets that did not react with the organic phase. The dispersion has higher tendency to dewet over the carbon grid than other imidized SMA/oil dispersions, likely due to some free oil as the hydrogenated oil has lowest reactivity among others.

The physical mixture of dispersed imidized SMA + MO was prepared as a reference. A two-phase mixture immediately formed when the oil was added (1:1 wt%) to a dispersion of pure imidized SMA. After moderately mixing with a magnetic stirrer for about 1 h, the mixture homogenized with a well-dispersed oil phase. The final viscosity (300 cp) was much higher than for pure imidized SMA and hybrid imidized SMA/oil nanoparticles, while the pH (=6.8) remained similar as for pure imidized SMA. It indicates by physical means that the oil remains free in the imidized SMA dispersion. The higher viscosity of physical mixtures is than likely caused by the intrinsic oil properties and molecular oil entanglements. The lower viscosity of chemically synthesized dispersions is than likely caused by (at least partial) incorporation and shielding of the oil by organic material. In parallel with the chemically synthesized dispersions, this physical mixture also remained stable for long times, as the imidized SMA has good surfactant properties. The Zeta-potential of physically mixed oil dispersions ($\zeta = -55$ mV) is in the range of pure imidized SMA and lower than the dispersions with chemically reacted hybrid nanoparticles.

Film-forming properties of nanoparticle dispersion

The film formation was characterized by optical microscopy in Fig. 3, including (i) pure imidized SMA, (ii) chemically synthesized dispersion of imidized SMA/MO, and (iii) physical mixture of imidized SMA + MO. The dispersions have suitable viscosities for processing, without thinning instabilities. The pure imidized SMA (Fig. 3a) forms a discontinuous film, as before on paper substrates (Samyn et al. 2010). The chemically imidized SMA/oil nanoparticles (Fig. 3b) form a more continuous film as the oil improves the flow properties and interactions of individual nanoparticles, while the tendency for dewetting reduces. The formation of a homogeneous film confirms that a one-phase dispersion was created, while the presence of oils have beneficial effect on binding of the single nanoparticles in the film. Indeed, the glass transition temperature of the hybrid nanoparticles is somewhat lower compared to the pure imidized SMA, while the better continuity also suggests that the interaction between nanoparticles may be influenced by some oil present at their surface. Later, we will further evaluate these films as possible barrier layers onto paper. After physically mixing pure imidized SMA + MO (Fig. 3c), a film with a fine (micron-scale) distribution of oil droplets into a polymer matrix develops. This morphology represents a two-phase dispersion that is stabilized by imidized SMA at the oil/water interface. This situation is different from the chemically synthesized imidized SMA/oil dispersions that forms a single-phase film. The possibility for physically mixing oil droplets into a water suspension, however, confirms that the presence of pure imidized SMA nanoparticles provides good dispersing properties.

FTIR spectroscopy of nanoparticles with different vegetable oils

Following phenomena were analyzed by FTIR: (i) interactions of hybrid nanoparticles in aqueous dispersion under different concentrations, (ii) characterization of bonding between oil and imidized SMA in dried or precipitated state.

First, the ATR-FTIR spectra for dispersed hybrid nanoparticles with different oils and fixed SC = 50 wt%, together with a reference sample of water and pure imidized SMA are shown in Fig. 4a and detailed in Fig. 4b. For oils, following bands represent the triacylglyceride groups (Samyn et al. 2012c): 2,937 cm^{-1} (asymmetrical C–H stretching), 2,856 cm^{-1} (symmetrical C–H stretching), 1,750 cm^{-1} (C=O stretching), 1,460 cm^{-1} (C–H scissoring), 1,166 cm^{-1} (C–O stretch and C–H bending), 709 cm^{-1} (C–H bending). For imidized SMA, following bands appear (Samyn et al. 2012a): 3,600–3,100 cm^{-1} (NH stretching vibrations); 3,100–2,990 cm^{-1} (St, C–H aromatic stretching); 2924, 2854 cm^{-1} (CH_2 in backbone chain); 1,950 cm^{-1} (St); 1860, 1780 cm^{-1} (C=O, anhydride ring); 1,710 cm^{-1} (N–C=O stretch, imide I); 1600, 1584 cm^{-1} (St, C=C stretch); 1493, 1453 cm^{-1} (St, aromatic C–C stretch); 1370, 1335 cm^{-1} (St, C–H aromatic vibrations), 1,345 cm^{-1} (imide II, C–N–C); 1220, 1090 cm^{-1}

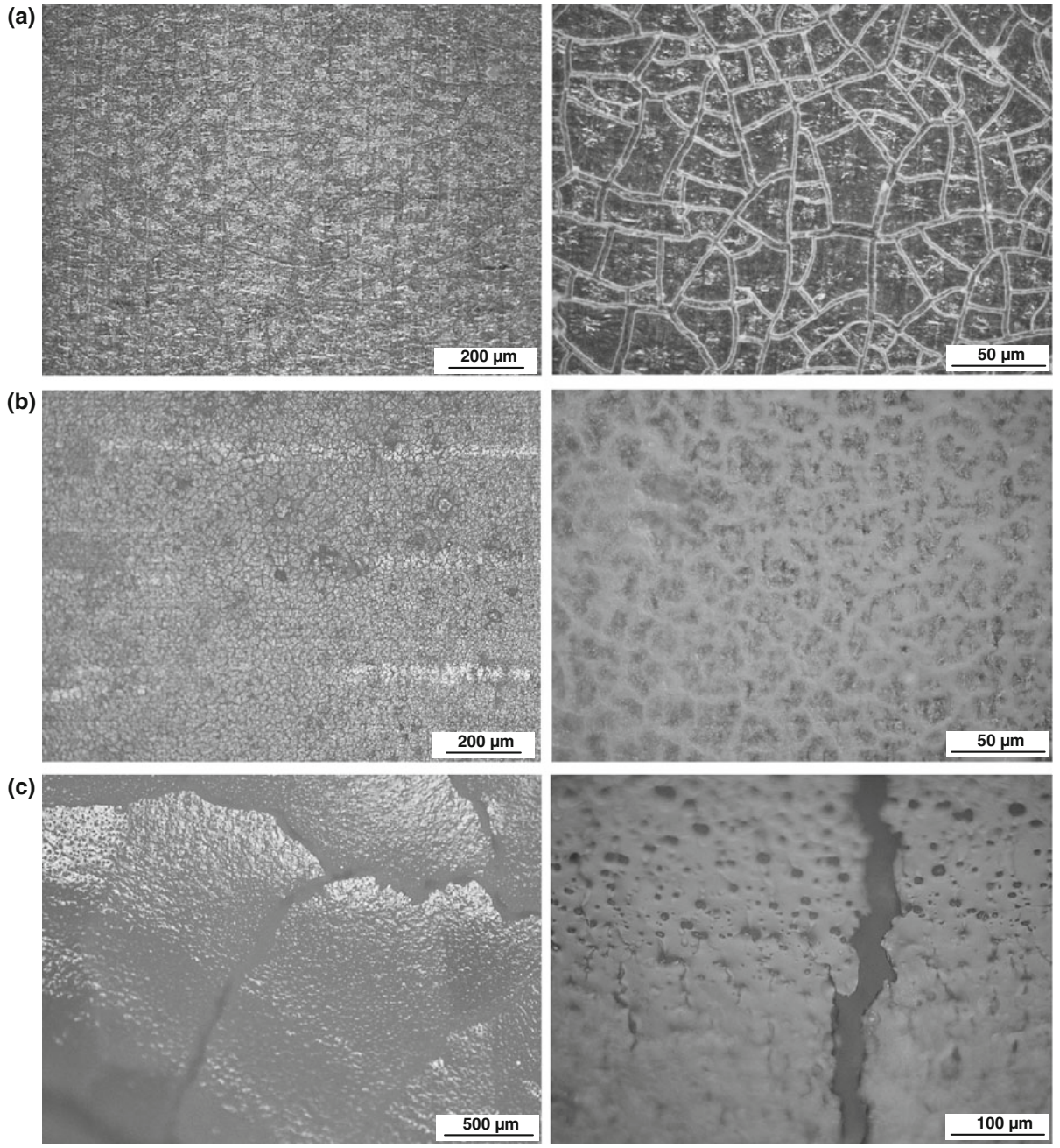

Fig. 3 Optical microscopy of films formed from aqueous nanoparticle dispersions after bar-coating onto aluminum foil, **a** pure imidized SMA, **b** chemically synthesized dispersions of imidized SMA/MO, **c** physically mixed dispersion imidized SMA + MO

(cyclic C–O–C and carbonyl, anhydride); 1,170 cm^{-1} (imide III); 1073, 1029, 907, 845, 757 and 695 cm^{-1} (St, aromatic C–H); 946–920 cm^{-1} (C–H vibration in cyclic carbonyl compounds, anhydride). All spectra are normalized on the St band (1,493 cm^{-1}). The dispersing water phase is seen as a broad band around 1,640 cm^{-1}. The imide peak (1,710 cm^{-1}) is largest for pure imidized SMA and has lower intensity for imidized SMA/oil. The imide content is largest for hybrid nanoparticles with SO, and progressively decreases with MO, KO, ZO, CO, and HCO. The oils interfere with completion of imidization and likely

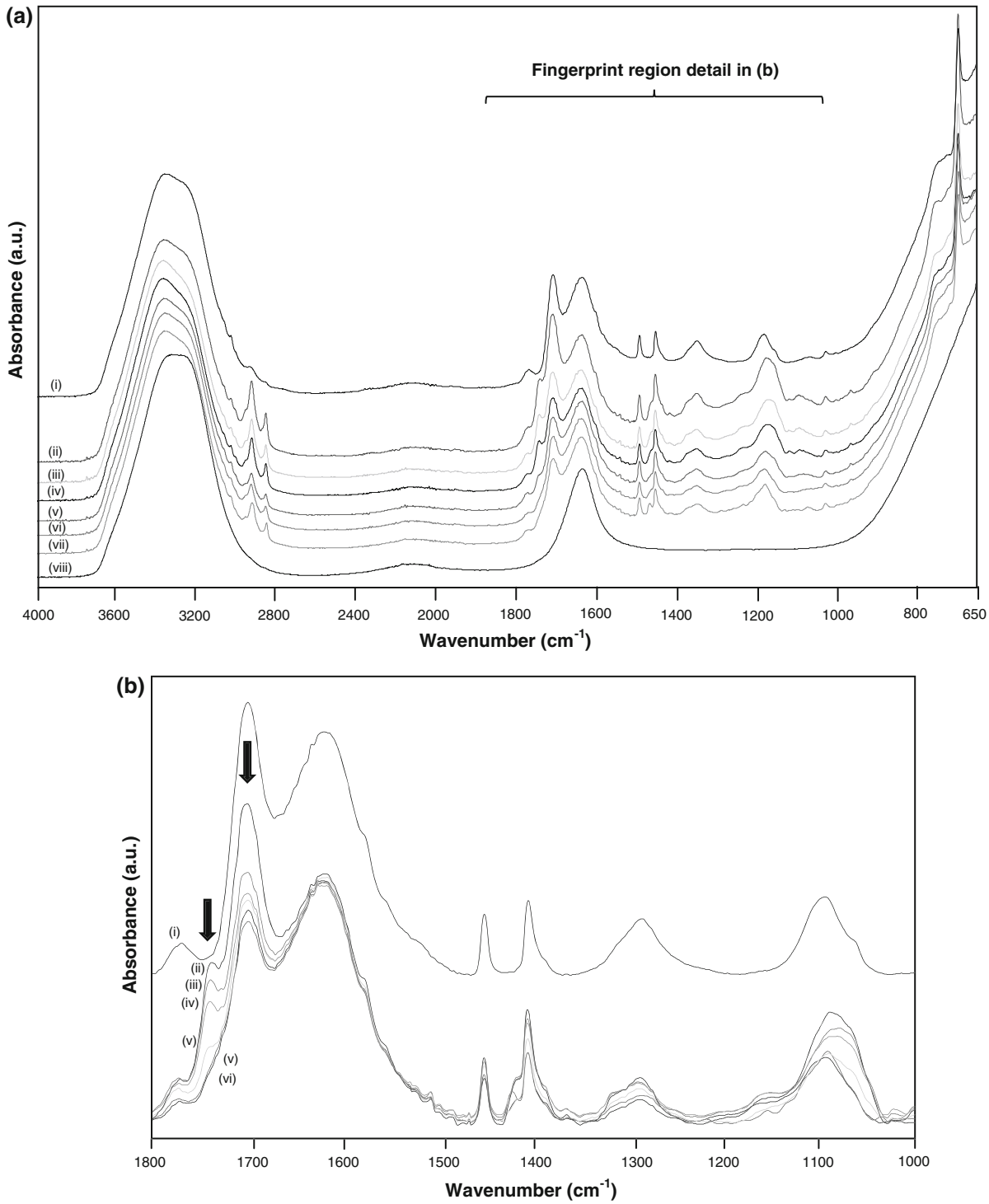

Fig. 4 ATR-FTIR analysis of hybrid nanoparticle dispersions in aqueous environment, including different oils with (*i*) pure imidized SMA, (*ii*) imidized SMA/SO, (*iii*) imidized SMA/MO, (*iv*) imidized SMA/KO, (*v*) imidized SMA/ZO, (*vi*) imidized SMA/CO, (*vii*) imidized SMA/HCO, (*viii*) pure water: **a** complete spectral range, and **b** overlap detail of fingerprint region

reduce the ring-closing reaction through adsorption near carboxylic moieties. The amount of remaining ring-opened anhydrides (1,780 cm^{-1}) is larger for pure imidized SMA and decreases in intensity for hybrid nanoparticles with SO, MO, KO, ZO, CO, and HCO. This ring-opened anhydride fraction explains the negative Zeta-potential and ensures good dispersion stability of the nanoparticles. The imide fraction increase with lower amounts of carboxylic groups, as the ring-opened anhydride also interacts with oils in a portion depending on the oil reactivity, i.e., SO has highest and HCO has lowest reactivity. The St band (1,493 cm^{-1}) is relatively constant, but some variations at 1,453 cm^{-1} occur through reorientation of the hydrophobic St ring toward the oil. This St-related band also overlaps with a C–H oil-related band (1,460 cm^{-1}), appearing as a shoulder with high intensity for SO, MO, KO, ZO, a shoulder with low intensity for CO, or even a separate band for HCO (the C–H amount indeed increases after hydrogenation). Another oil-related band (1,750 cm^{-1}) also decreases in parallel with oil reactivity. The spectra for diluted dispersions with SC = 50–10 wt% in Fig. 5 show a linear in-/decrease for water-/imide-related bands, respectively. The oil-related bands decrease proportionally with imide-related bands, indicating no oil leakage from the organic phase. Thus, the dispersion may be diluted after reaction to tune the viscosity for appropriate processing (e.g., rheological behavior).

Second, the FTIR spectra of dried hybrid nanoparticles are shown in Fig. 6a and detailed in Fig. 6b. The absorption bands of the organic phase become sharper after water removal, while the oils remain included. Especially, the imide bands improve by ring-closing of anhydride moieties. However, the imide bands for hybrid nanoparticles ever remain smaller than for pure imidized SMA. The fraction of ring-opened anhydride moieties in carboxyl conformation (1,780 cm^{-1}) is highest for hybrid nanoparticles (due to oil interactions) and almost negligible for pure imidized SMA (higher imide content). The positions and intensities of St bands remain constant after drying, as the hydrophobic moieties are oriented toward the oil phase and do not re-orient relatively to the dispersed state. The spectra of precipitated hybrid nanoparticles in Fig. 7 indicate similar behavior of oil and organic phases as above. An additional absorption region at 1,650–1,500 cm^{-1} represents amic acid moieties (COOH/$CONH_2$), forming at low pH by protonation of ring-opened anhydride. This conversion reduces the negative charges around carboxylic groups (Zeta-potential −5 mV) and destroys the dispersion stability with consequent precipitation, while the oil phase is qualitatively not affected.

Specific interactions between the oil and organic phase are demonstrated in the FTIR spectra in Fig. 8a, by comparing pure MO, pure imidized SMA, and imidized SMA/MO. The interactions are localized around the imide-related C=O and C–N–C bands, which have lower intensity in hybrid nanoparticles than in pure imidized SMA as an indication for more ring-opened structures. The St moieties remain unchanged. The reactivity between different oils and the polymer phase is best seen from Fig. 8b, with low imide intensities and splitting of the C=O band into separate components depending on the oil type: most interactions happen with unsaturated oil types while only small interactions happen with HCO. The lower imidization in the presence of oils is also confirmed by a remaining fraction of cyclic C–O–C anhydride groups (1,850 cm^{-1}), which had completely disappeared for pure imidized SMA. The intensity of St rings (1,950 cm^{-1}) is lower for hybrid nanoparticles than for pure imidized SMA and has about similar intensity for all oils types: this represents re-orientation and rotation of the St parts independently of the oil type.

The discussions illustrate the interactions of different oil types with imidized SMA, but a quantitative analysis from FTIR spectra cannot be made due to band overlap and conformation sensitivity.

FT-Raman spectroscopy of nanoparticles with different vegetable oils

Following phenomena were analyzed by FT-Raman: (i) quantitative analysis of imide content and oil reactivity, (ii) oil conformation, (iii) interactions between oils and imidized SMA, (iv) effects of physically mixed oil into pure imidized SMA dispersion and chemically imidized SMA/oil.

First, the FT-Raman spectra of dispersed and dried hybrid nanoparticles are shown in Fig. 9. The spectra of precipitated nanoparticles were similar to the dried ones and are not shown. The oils are characterized by Samyn et al. (2012c): 3,010 cm^{-1} (symmetric = C–H stretching), 2,909 cm^{-1} (C–H stretching), 2,880 (aliphatic CH stretching of $–CH_2$ and $–CH_3$), 2,885 cm^{-1}

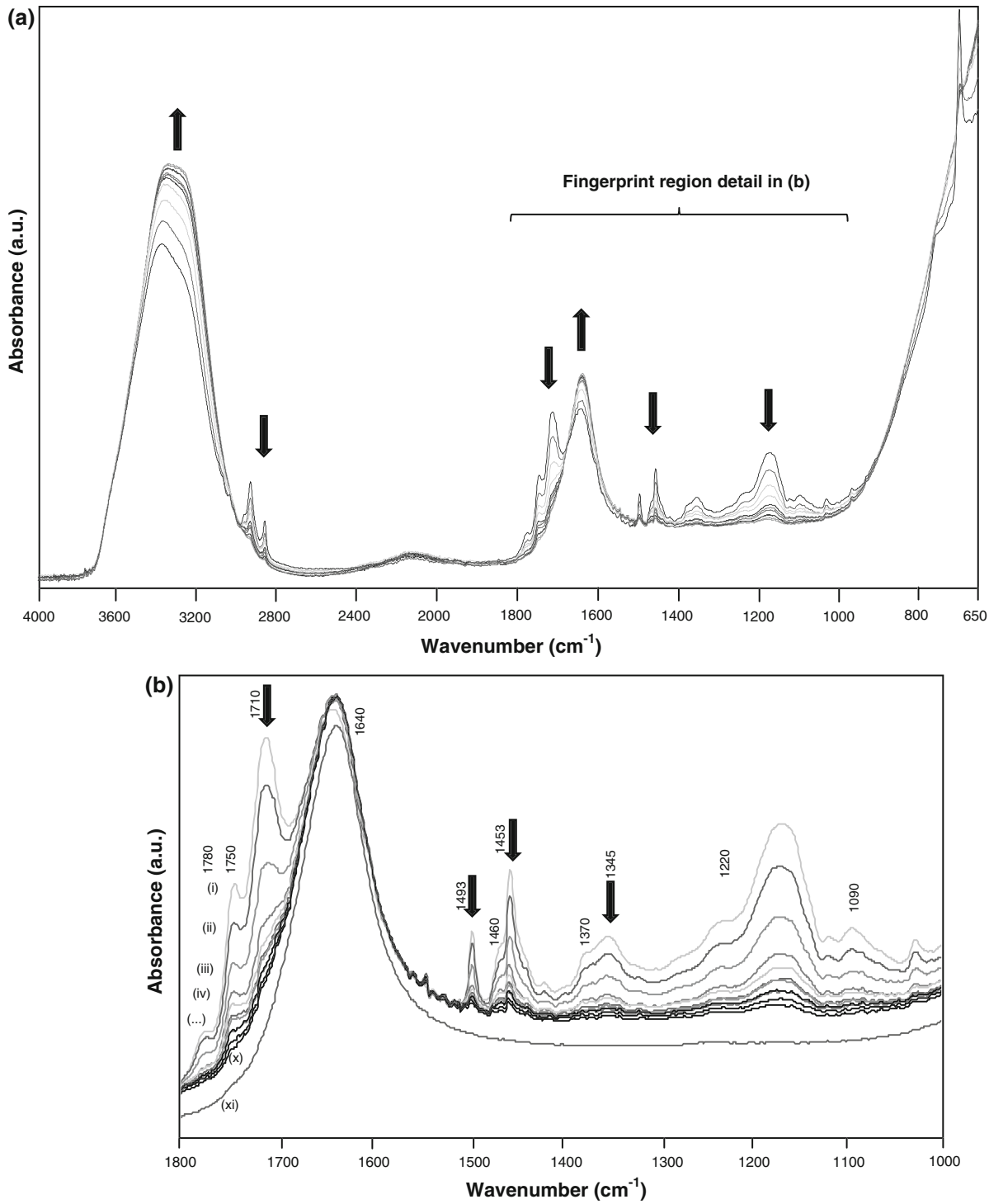

Fig. 5 ATR-FTIR analysis of hybrid nanoparticle dispersions in aqueous environment with dilutions from SC = 50 to 0.10 wt%, including (*i*) 50 wt%, (*ii*) 25 wt%, (*iii*) 12.5 wt%, (*iv*) 6.25 wt%, (*v*) 3.52 wt%, (*vi*) 1.56 wt%, (*vii*) 0.78 wt%, (*viii*) 0.39 wt%, (*ix*) 0.20 wt%, (*x*) 0.10 wt%, (*xi*) pure water: **a** complete spectral range, and **b** overlap detail of fingerprint region

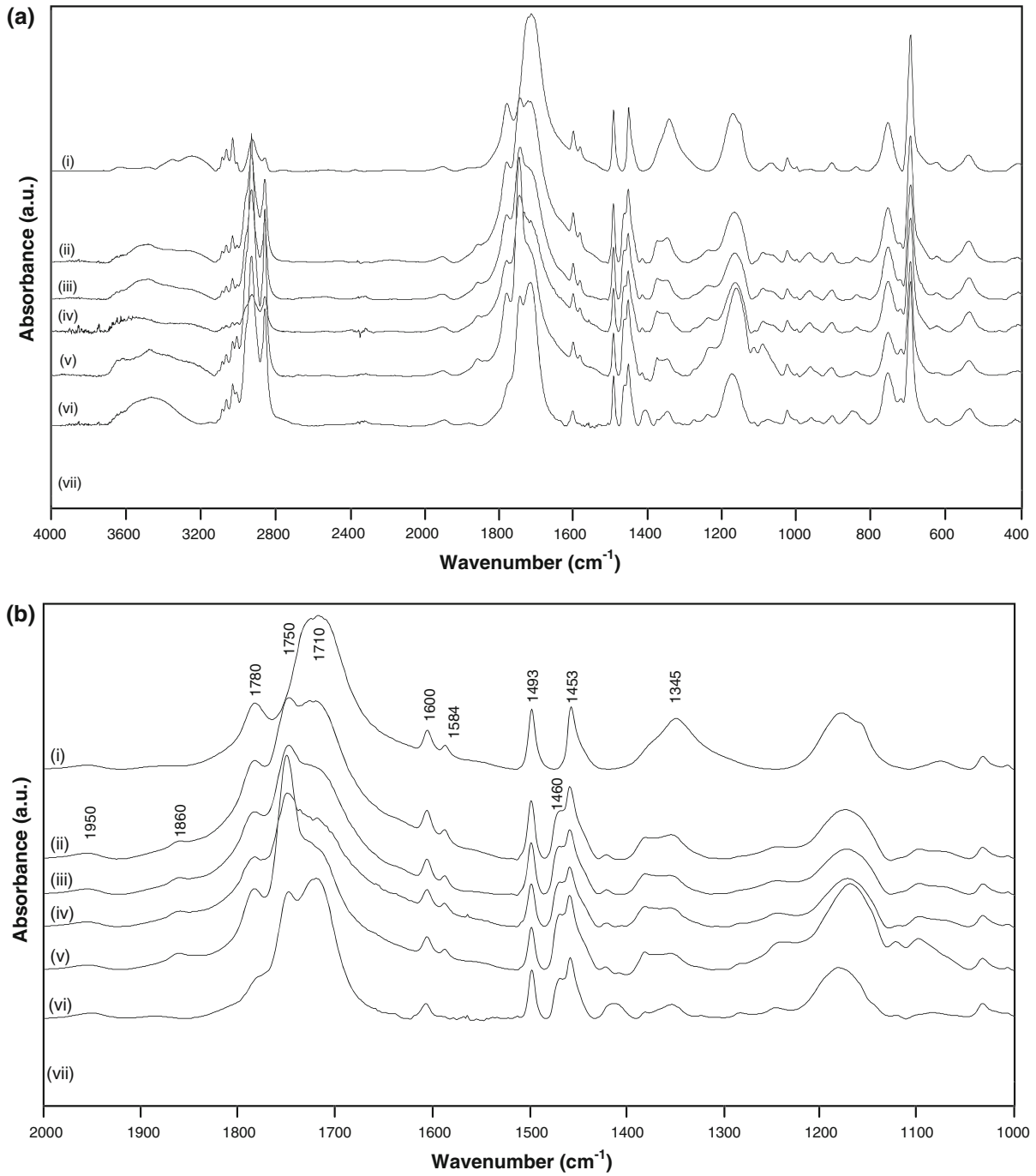

Fig. 6 FTIR analysis of hybrid nanoparticles after drying, including different oils with (*i*) pure imidized SMA, (*ii*) imidized SMA/SO, (*iii*) imidized SMA/MO, (*iv*) imidized SMA/KO, (*v*) imidized SMA/ZO, (*vi*) imidized SMA/CO, and (*vii*) imidized SMA/HCO

(symmetric aliphatic C–H), 1,746 cm^{-1} (ester *v*(C=O) stretching), 1,660 cm^{-1} (*cis* C=C stretching), 1,442 cm^{-1} (δ-CH_2 scissoring deformation), 1,305 cm^{-1} (γ-CH_2 in phase twisting), 1,266 cm^{-1} (=C–H in-plane bending in unconjugated *cis* double bond), 1,100–1,000 cm^{-1} (–$(CH_2)_n$—deformation), and 900–800 cm^{-1} (CH_2 twisting and rocking). The imidized SMA is characterized by Samyn et al.

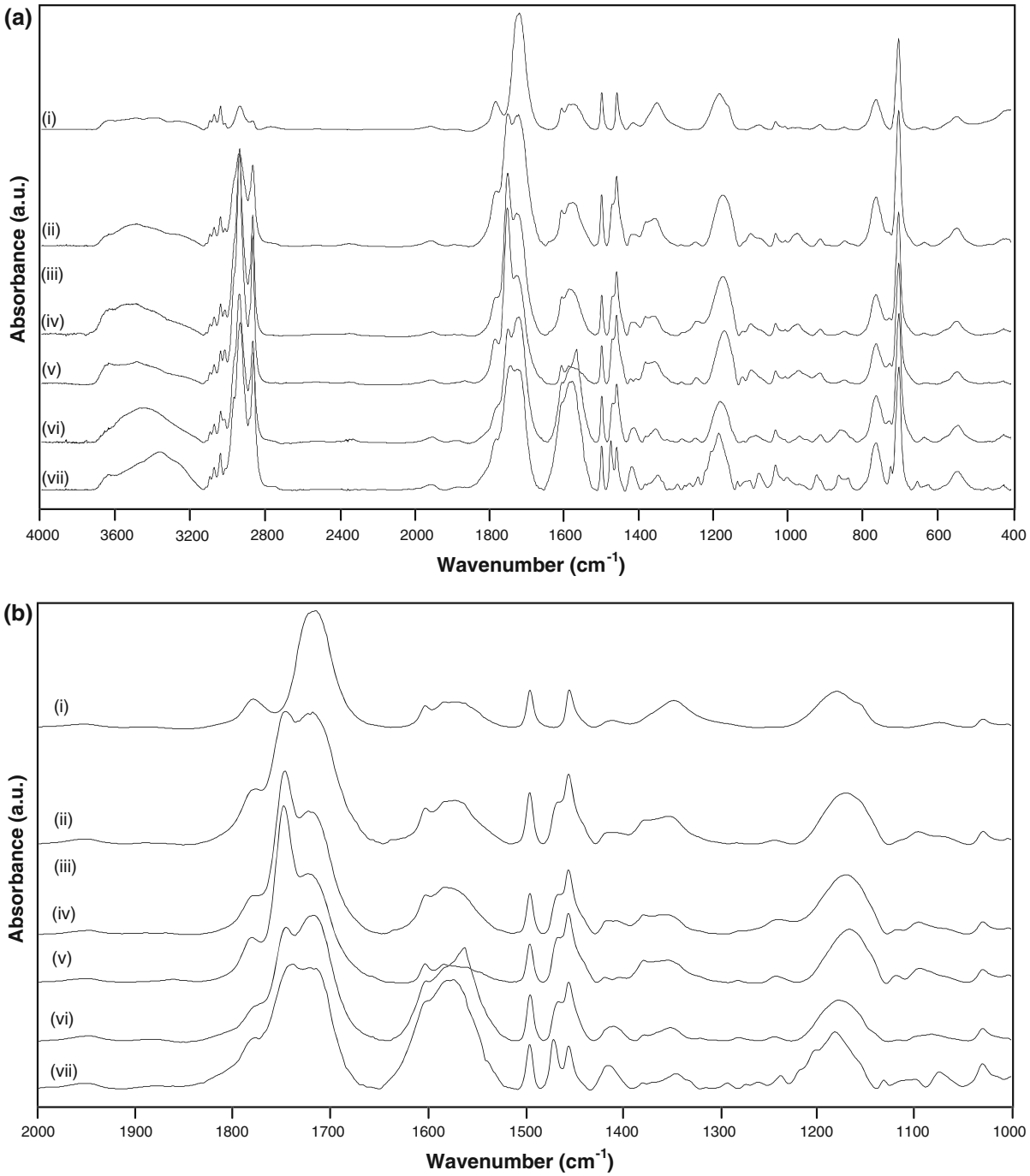

Fig. 7 FTIR analysis of hybrid nanoparticles after precipitation, including different oils with (*i*) pure imidized SMA, (*ii*) imidized SMA/SO, (*iii*) imidized SMA/MO, (*iv*) imidized SMA/KO, (*v*) imidized SMA/ZO, (*vi*) imidized SMA/CO, and (*vii*) imidized SMA/HCO

(2012a): 3,059 cm^{-1} (St, CH_2); 2,916 cm^{-1} (CH_2 backbone); 1,860 cm^{-1} (C=O, anhydride); 1,765 cm^{-1} (C=O, imide I); 1602, 1585, 1452 cm^{-1} (St, aromatic C=C); 1,329 cm^{-1} (C–N–C, imide II); 1184, 1156, 1031, 1000, 794, 620 cm^{-1} (St). All spectra are normalized on the St band (1,602 cm^{-1}).

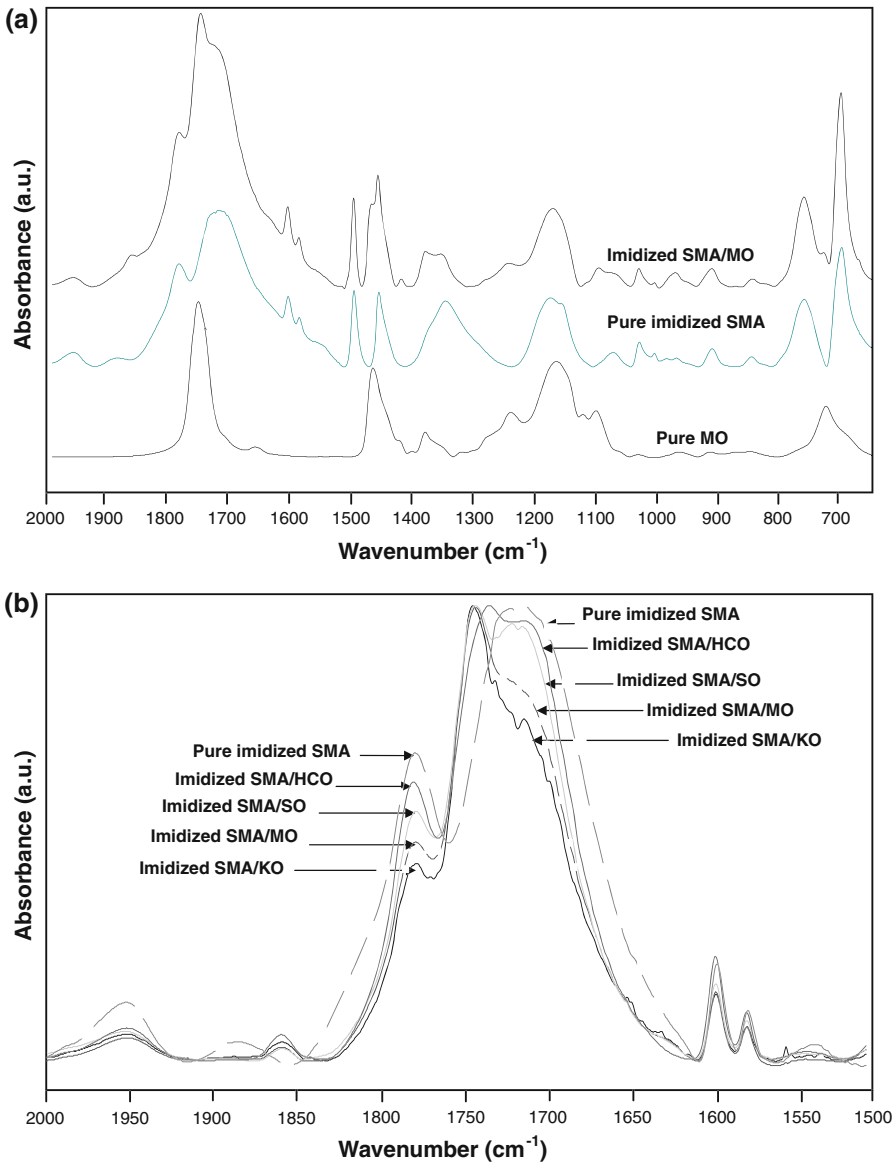

Fig. 8 Detailed FTIR analysis representing interactions between oil and organic phase in **a** hybrid organic nanoparticles with imidized SMA/MO, **b** hybrid nanoparticles with different oils

The spectra for water-dispersed nanoparticles (Fig. 9a) have contributions of hydroxyl stretching (3,100–3,400 cm^{-1}) and H–O–H bending vibration (weak 1,630 cm^{-1} band). The latter do not interfere with imidized SMA or oil bands, and disappear after drying (Fig. 9b). The imide content can be calculated from ratioing the peak areas of the imide I (1,765 cm^{-1}) and St band (1,602 cm^{-1}), after calibration with a fully imidized sample prepared by heating for 6 h at 250 °C (Samyn et al. 2012a). Those values are given in Table 3, compared to a theoretical maximum imide content (relatively to St parts) of 35 %. The imide contents of dried nanoparticles is higher than dispersed ones, as the drying induces further condensation of ammonolyzed anhydride moieties into ring-closed imide. The imide content of imidized SMA/oil nanoparticles (26–19 % after drying) is lower than pure imidized SMA (29 % after drying). Indeed, some ring-opened anhydrides likely react with fatty acids and are prevented to transform into imides in the presence of oil. In parallel, a small remaining fraction of anhydride for dried nanoparticles is observed at 1,860 cm^{-1} (Fig. 9b): the C=O in cyclic anhydride is more prominent for imidized

SMA/oil than for pure imidized SMA. These observations illustrate chemical coupling between oils and organic phase through esterification near the anhydrides. The imide content of hybrid nanoparticles depends on the oil type, with 23–26 % in the presence of poly-unsaturated oils (SO, MO), 19–21 % for mono-unsaturated oils (KO, ZO, CO) and 24 % for saturated oils (HCO). The high imide content for imidized SMA/HCO indicates very little interactions between oil and organic phase and consequently little disturbance of the imidization reaction. The reactivity of different oils interacting with the organic phase thus mainly depends on its degree of saturation, with poly-unsaturated oils the most reactive and saturated oils

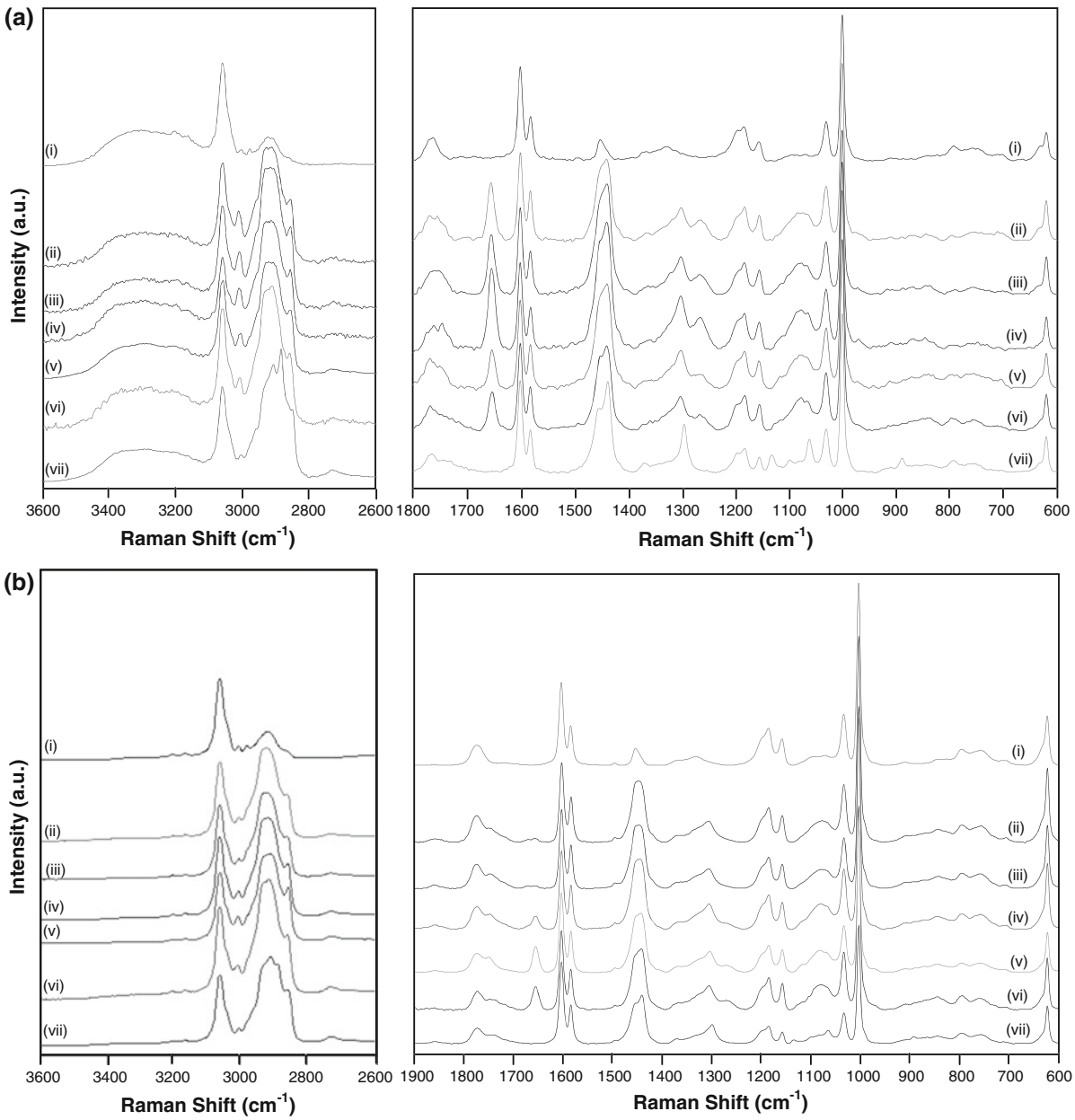

Fig. 9 Raman analysis of hybrid organic nanoparticles **a** in dispersion, and **b** after drying including different oils with (*i*) pure imidized SMA, (*ii*) imidized SMA/SO, (*iii*) imidized SMA/MO, (*iv*) imidized SMA/KO, (*v*) imidized SMA/ZO, (*vi*) imidized SMA/CO, and (*vii*) imidized SMA/HCO

Table 3 Imide content and reacted oil content for hybrid organic nanoparticles with imidized SMA/oil

Nanoparticle type	Imide content in aqueous dispersion (%)	Imide content after drying (%)	Reacted oil content[a] (%)	Free oil content[a] (%)
Imidized SMA	24	29	–	–
Imidized SMA/SO	20	26	96	4
Imidized SMA/MO	18	23	95	5
Imidized SMA/KO	16	21	85	15
Imidized SMA/ZO	15	19	78	22
Imidized SMA/CO	14	19	76	24
Imidized SMA/HCO	17	24	Cannot be defined[a]	

[a] Based on C=C as reactive sites

the less reactive. The oil reactivity is also confirmed by the *cis* C=C conformation band (1,660 cm^{-1}), which almost disappears after drying hybrid nanoparticles with polyunsaturated oils, but remains present for mono-unsaturated oils. The reacted oil content is also calculated in Table 3, assuming that the C=C bonds are reactive sites: the double bonds almost completely reacted for SO and MO, while some unreacted ones are seen for KO, ZO, and CO. From the spectra under dispersed (Fig. 9a) and dried conditions (Fig. 9b), the *cis* C=C bonds exist in aqueous medium while coupling and/or reorientation between oil and organic phase mainly builds under drying. The oil reactivity agrees with a qualitative trend in bending bands of unconjugated *cis* double bonds (1,266 cm^{-1}). All these observations illustrate certain mobility of the oil relatively to the organic phase, which is lower for dried hybrid nanoparticles in parallel with a lower intensity of δ-CH_2 scissoring bands (1,442 cm^{-1}). We hypothesize that the variations in oil conformation and/or interactions under dispersed and dry conditions are caused by an "oil drag" around the nanoparticles. This interestingly explains that nanoparticle diameters according to DLS are about 130–150 nm (wet), while they are about 20–50 nm according to TEM (dried).

Second, the C=C conformation in dispersed and dried hybrid nanoparticles is detailed in Fig. 10. This region (1,660 cm^{-1}) relates to saturation and conformation of oils, allowing to estimate the degree of unsaturation depending on frequency positions (Sadeghi-Jorabchi et al. 1991): the intensity maximum for polyunsaturated fatty acids (1,657 cm^{-1}) is higher than for mono-unsaturated fatty acids (1,655 cm^{-1}). Indeed, this band has multiple maxima toward the high end for SO, MO and the low end for KO, ZO, CO, and HCO. The typical *trans* isomeric band (1,680–1,670 cm^{-1}) does not appear in pure oils (Samyn et al. 2012c), except in very small amounts for HCO through hydrogenation. The C=C in pure vegetable oils have indeed *cis* conformation as most natural appearance (Sadeghi-Jorabchi et al. 1991). After incorporation in the hybrid nanoparticles and drying (Fig. 10b), the peak maxima related to poly-unsaturated fatty acids at higher Raman shifts decrease somewhat in intensity and a *trans*-band (1,680–1,670 cm^{-1}) gradually appears. The latter suggests that the fatty acid conformation slightly rearranges from *cis* into *trans* for imidized SMA/oil. The intensity of the *trans*-band is highest for SO and MO as the reorientation mainly develops for most reactive oils with originally highest degree of unsaturation (IV).

Third, the C=O interactions around acid moieties of organic and oil phases (1,800–1,700 cm^{-1}) are detailed in Fig. 11. The interactions in dispersion (Fig. 11a) are again more complex than after drying (Fig. 11b). A broad range of C=O conformations for ammonolyzed SMA indicates ring-opened and partly ring-closed conformations in dispersion, which develop into a permanent imide conformation after drying. The interactions of ring-opened C=O with the oil phase are instable while the oil still seems to form a separate phase in the dispersion. A shift in C=O band between dispersed (1,765 cm^{-1}) and dried (1,770 cm^{-1}) state, indicates the progress of imidization. On the other hand, the position of the fatty acid C=O band remains relatively fixed (1,746–1,748 cm^{-1}), as an indication that they are less reactive than the C=C in oil. The IV for pure oils (see also Table 1) could be directly calculated from Raman spectra, as before (Samyn et al. 2012c). The IV calculation after chemical reaction is difficult due to interactions with imide-related absorption bands, but a

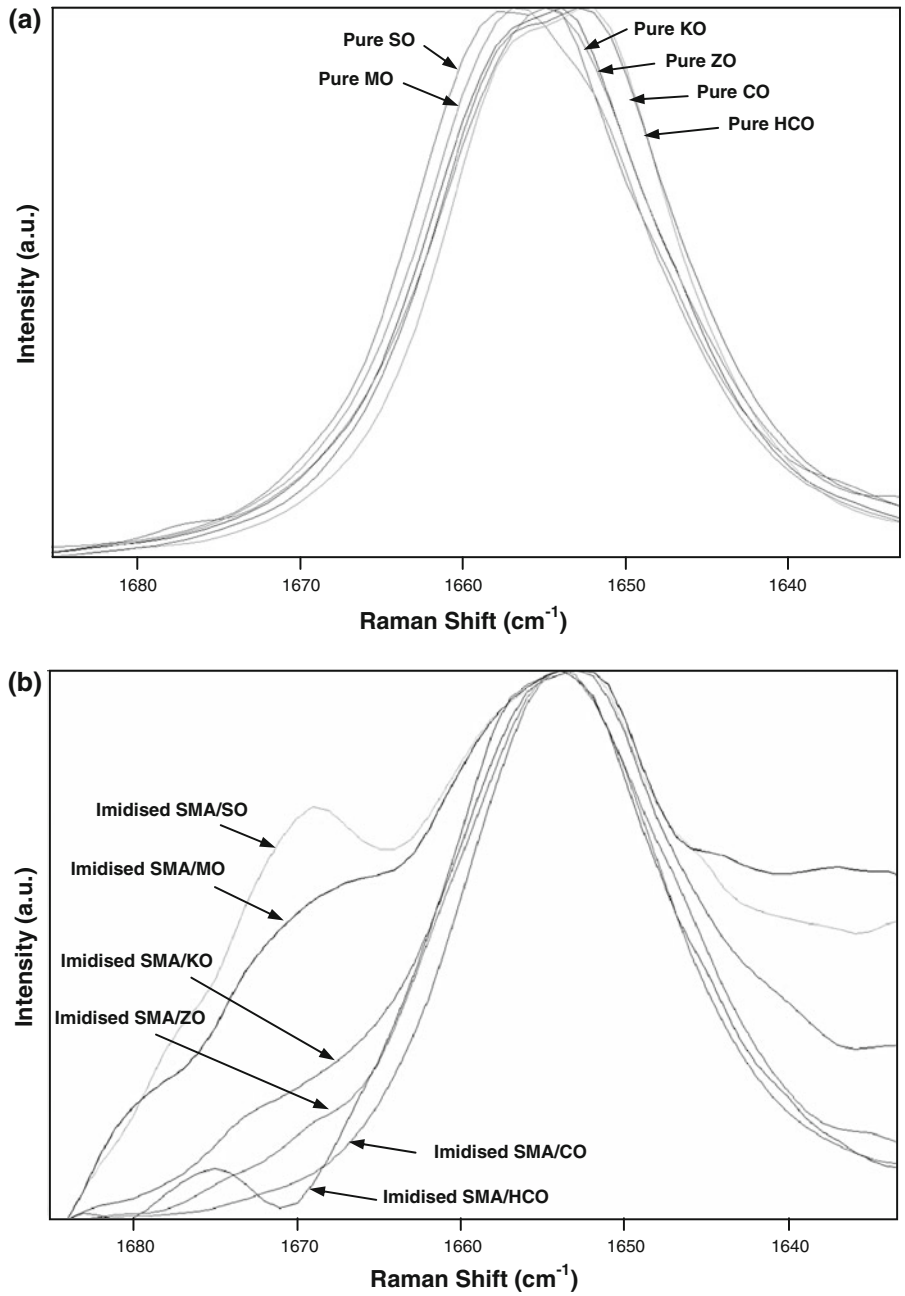

Fig. 10 Detailed Raman analysis of the oil phase behavior in hybrid organic nanoparticles **a** pure oils, **b** oils incorporated in imidized SMA nanoparticles after drying

qualitative classification indicates increasing IV after reaction, as follows: HCO, MO, SO, CO, ZO, and KO. This order differs from pure oils, as the reacted SO, MO (poly-unsaturated) significantly reduced in IV due to high reactivity at C=C bonds, while KO, ZO (mono-unsaturated) retain a relatively high IV due to lower reactivity.

Finally, pure MO, pure imidized SMA, imidized SMA/MO hybrid nanoparticles and a physical mixture of pure imidized SMA + MO in dispersion are compared in Fig. 12. The spectrum of chemically synthesized hybrid organic nanoparticles cannot be seen as a pure sum of its components due to supplementary interactions (Fig. 12a). For pure oils,

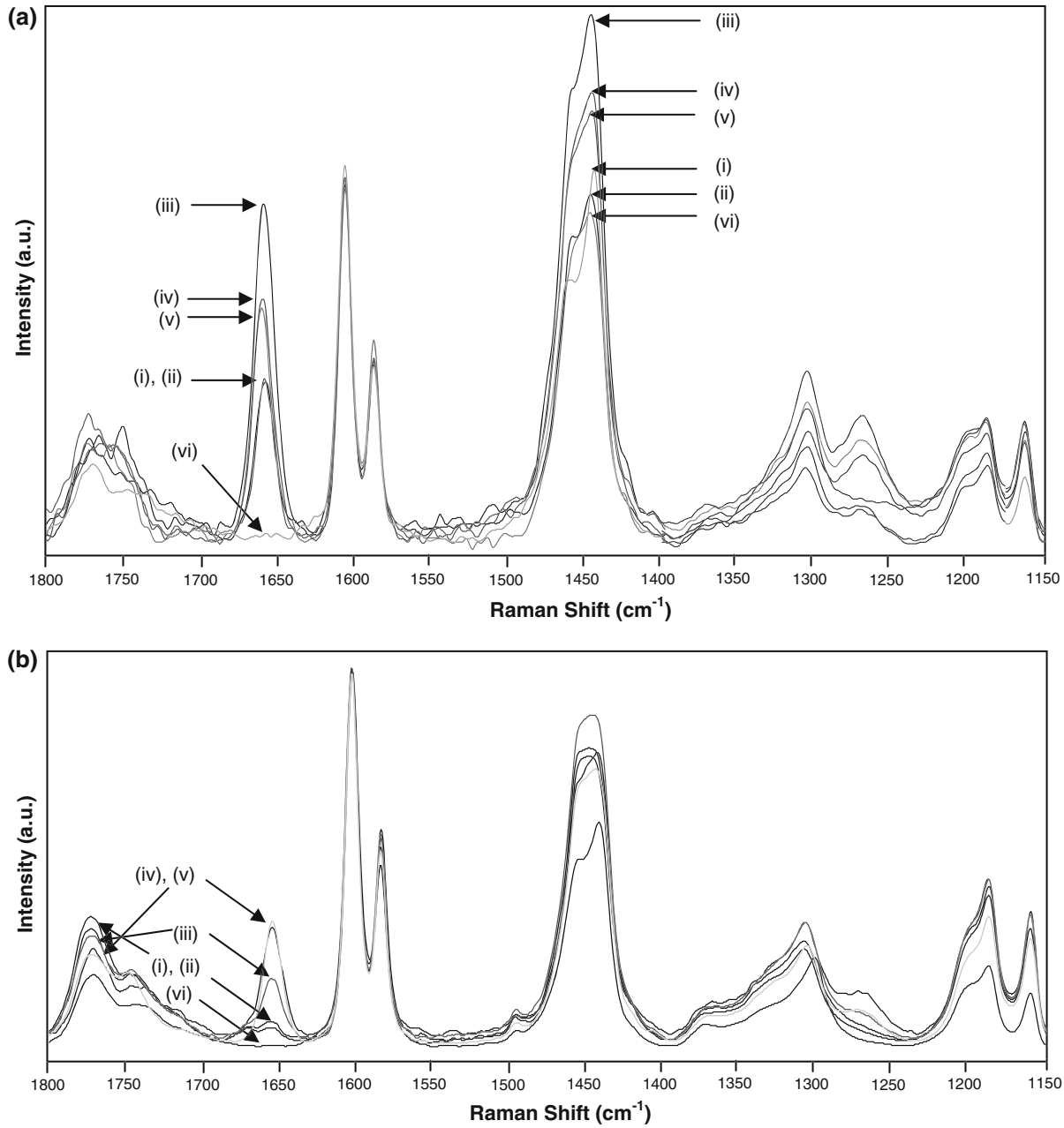

Fig. 11 Detailed Raman analysis of hybrid organic nanoparticles **a** in dispersion, and **b** after drying including different oils with (*i*) imidized SMA/SO, (*ii*) imidized SMA/MO, (*iii*) imidized SMA/KO, (*iv*) imidized SMA/ZO, (*v*) imidized SMA/CO, and (*vi*) imidized SMA/HCO

the absorption peak at 3,010 cm^{-1} is due to C–H stretching vibrations of hydrogen atoms bonded to certain types of sp^2 carbon atoms (Muik et al. 2005), and indirectly related to the number of double bonds (Baeten 1996). The qualitative reduction in number of double bonds in hybrid organic nanoparticles of imidized SMA/MO confirms previous discussions. Although the St moieties (1,602 cm^{-1}) are chemically inert, another St band (1,000 cm^{-1}) is different for pure imidized SMA and imidized SMA/MO. These variations are related to orientation effects for which the 1,000 cm^{-1} is more sensitive: the orientation of St

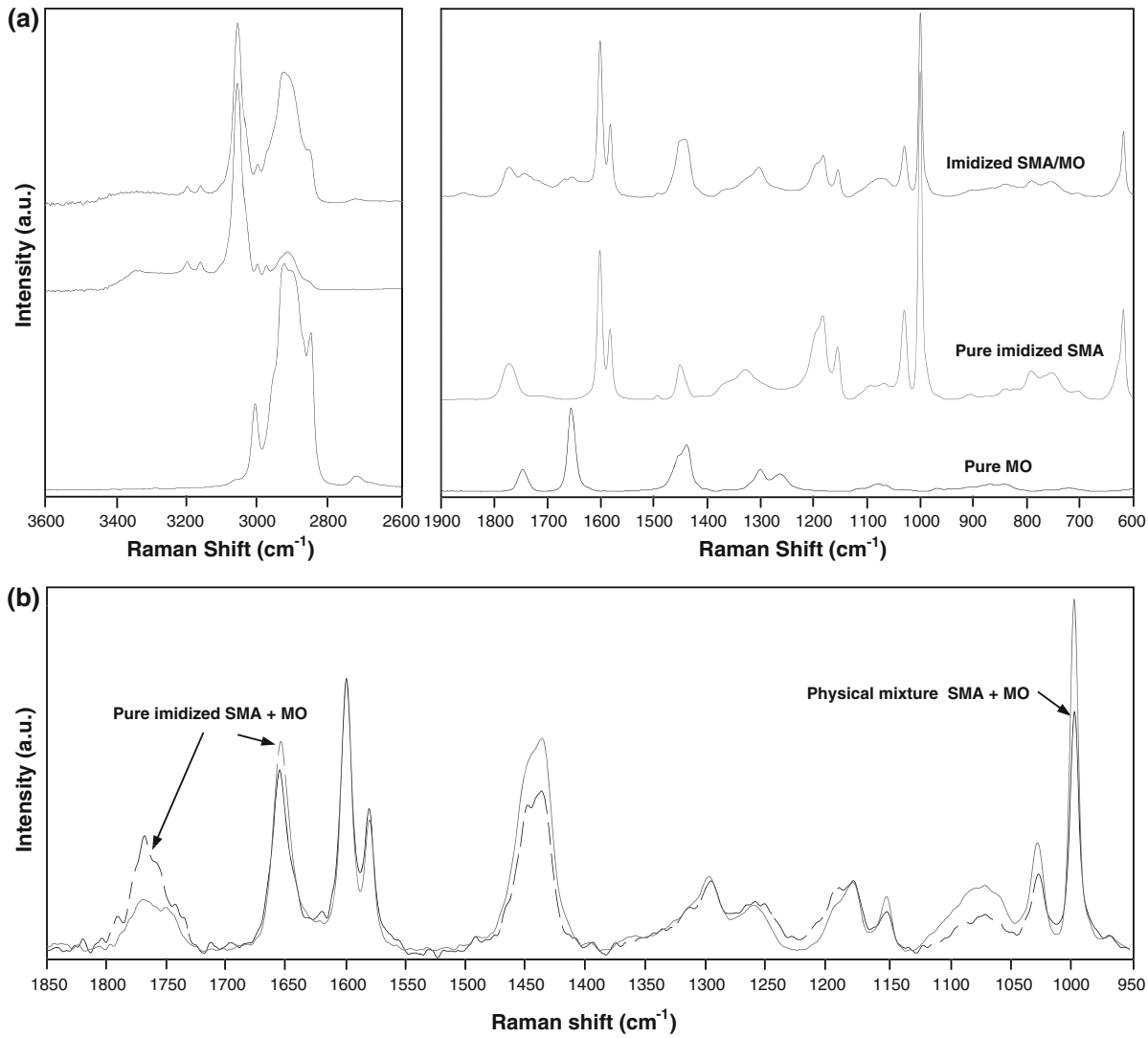

Fig. 12 Detailed Raman analysis representing interactions **a** between oil and organic phase in hybrid organic nanoparticles with imidized SMA/MO (dried), **b** between chemically synthesized imidized SMA/Mo and physical mixture of imidized SMA + MO (both in dispersion)

moieties in the presence of oil is more confined, as they likely orient toward the oil droplets while being more random in the absence of oil. This confinement may also affect the re-orientation of the CH_2 functions, as the γ-CH_2 in phase twisting (1,305 cm^{-1}) disappears while the overall $(CH_2)_n$ (1,100–1,000 cm^{-1}) exists in the hybrid organic nanoparticles. On the other hand, the broad C=O absorption region for hybrid organic nanoparticles suggests the formation of C=O dimer structures between the oil and organic phase. The chemical synthesis of imidized SMA/MO and physical mixture of imidized SMA + MO are compared in Fig. 12b, with main spectral differences at the C=O imide peak (1,765 cm^{-1}) and St peak (1,100 cm^{-1}). The imide structure of physical mixtures is identical to pure imidized SMA nanoparticles, with higher contents than for hybrid organic nanoparticles. This indicates that there is no chemical binding between polymer and oils for physical mixtures. The orientation of the St depends on the oil environment which is either chemically or physically bonded to the polymer phase. The physically mixed oil has more

double bonds than chemically reacted oils, as it retains its original characteristics without chemical coupling to the organic phase.

Conclusions

Hybrid organic nanoparticles were synthesized by adding vegetable oils to the imidization reaction of SMA with ammonium hydroxide in aqueous environment. The imidization reaction was positively influenced by oils, as the maximum viscosity of the reaction mixture decreased depending on the oil type, the time for termination shortened, and the maximum solid content of the reaction mixture increased to at least 50 wt% compared with 35 wt% for pure imidized SMA. The dispersions have good stability at pH $>$ 4, confirmed by Zeta-potential measurements and favorable viscosity to form continuous bar-coated films. No leakage of oil was observed after dilution or pH variation.

The morphology of imidized SMA/oil nanoparticles changes with oil type, having homogeneous spherical shapes (diameter 20–60 nm) for poly-unsaturated oils, core–shell shapes (shell 5–7 nm) for mono-unsaturated oils, or containing free oil for the most saturated oils.

From spectroscopic analysis, the main interactions between oil and organic phases occur at unsaturated C=C bonds and ammonolyzed anhydride parts. As such, the poly-unsaturated oils (SO or MO) are more reactive than mono-unsaturated oils (rapeseed, sunflower, castor), and hydrogenated oils are less reactive. After reaction into hybrid nanoparticles, the fatty acid conformation slightly rearranges from *cis* into *trans* conformation. The reacted oil contents were quantified by Raman analysis, together with calculation of imide contents. As such, the imide content for hybrid organic nanoparticles is lower than for pure imidized SMA nanoparticles, while a remaining fraction of ammonolyzed anhydride provides good dispersion stability. The imide content is highest for particles with poly-unsaturated oils and decreases for mono-unsaturated ones. The imide content further increases after drying from the dispersion phase, or it forms amic acid complexes after precipitation at pH $<$ 4. The behavior of oil and organic phases during chemical synthesis were confirmed by a reference experiment with physically mixed imidized SMA + oil, where lower interactions were observed. The oils likely reduce the final imide content through adsorption at ammonolyzed anhydride parts.

Acknowledgments H. Van den Abbeele and G. Schoukens thank the Institute for the Promotion of Innovation by Science and Technology in Flanders (I.W.T.) for a funding program "SNAP" (contract grant IWT-080213). P. Samyn acknowledges the Robert Bosch Foundation for support in the Junior Professorship Program "Sustainable use of Natural Resources." We thank Dr. Ralf Thomann for TEM analysis.

References

Abang S, Chan ES, Poncelet D (2012) Effects of process variables on the encapsulation of oil in alginate capsules using an inverse gelation technique. J Microencapsul. doi: 10.3109/02652048.2012.655331

Adamiec J, Marciniak E (2004) Microencapsulation of oil/matrix/water system during spray drying process. In: Drying 2004, proceedings of the 14th international drying symposium, Sao Paulo, Brazil, pp 2043–2050

Alkan C, Sari A, Uzun O (2006) Poly(ethylene glycol)/acrylic polymer blends for latent heat thermal energy storage. J Am Inst Chem Eng 52:3310–3314

Bae KH, Lee Y, Park TG (2007) Oil-encapsulating PEO–PPO–PEO/PEG shell cross-linked nanocapsules for target-specific delivery of paclitaxel. Biomacromolecules 8:650–656

Baeten V, Meurens M (1996) Detection of virgin olive oil adulteration by Fourier Transform Raman Spectroscopy. J Agric Food Chem 44:2225–2230

Braun D, Sauerwein R, Hellmann GP (2001) Polymeric surfactants from styrene-co-maleic anhydride copolymers. Macromol Symp 163:59–66

Calvo P, Hernandez T, Lozano M, Gonzalez-Gomez D (2010) Microencapsulation of extra-virgin olive oil by spray-drying: influence of wall material and olive quality. Eur J Lipid Sci Technol 112:852–858

Domian E, Wqsak I (2008) Encapsulation of rapeseed oil based on spray drying method. Pol J Food Nutr Sci 58:477–483

Esumi K (2003) Dendrimers for nanoparticle synthesis and dispersion stabilization. Top Curr Chem 227:31–52

Fairhurst D, Loxley A (2008) Micro- and nano-encapsulation of water- and oil-soluble actives for cosmetic and pharmaceutical applications. In: Wiechers JW (ed) Science and applications of skin delivery systems. Allured Publishing, Carol Stream, pp 313–336

Frere W, Danchier L, Gramain P (1998) Preparation of microcapsules by interfacial polymerization. Eur Polym J 34:193–199

Fuchs M, Turchiuli C, Bohin M, Cuvelier ME, Ordonnaud C, Peyrat-Maillard MN, Dumoulin E (2006) Encapsulation of oil in powder using spray drying and fluidised bed agglomeration. J Food Eng 75:35–37

Glenn GM, Klamczynski AP, Woods DF, Chiou BS, Orts WJ, Imam SH (2010) Encapsulation of plant oils in porous starch microspheres. J Agric Food Chem 58:4180–4184

Hawlader MNA, Uddin MS, Khin MM (2003) Microencapsulated PCM thermal-energy storage system. Appl Energy 74:195–202

Hong Y, Xin-shi G (2000) Preparation of polyethylene–paraffin compound as a form-stable solid–liquid phase change material. Sol Energy Mater Cells 64:37–44

Horie M, Yanagisawa H, Sugawara M (2007) Fluorometric immunoassay based on pH-sensitive dye-encapsulating liposomes and gramicidin channels. Anal Biochem 369:192–201

Hsieh WC, Chang CP, Gao YL (2006) Controlled release properties of chitosan encapsulated volatile citronella oil microcapsules by thermal treatments. Colloid Surf B 53:209–214

Inaba H, Tu P (1997) Evaluation of thermophysical characteristics on shape-stabilized paraffin as a solid–liquid phase change material. Heat Mass Transf 32:307–312

Jafari SM, Assadpoor E, He Y, Bhandari B (2008a) Encapsulation efficiency of food flavours and oils during spray drying. Dry Technol 26:816–835

Jafari SM, Assadpoor E, Bhandani Y, He Y (2008b) Nanoparticle encapsulation of fish oil by spray drying. Food Res Int 41:172–183

Jovanovic AV, Underhill RS, Bucholz TL, Duran RS (2005) Oil core and silica shell nanocapsules: towards controlling the size and the ability to sequester hydrophobic compounds. Chem Mater 17:3375–3383

Kim EY, Kim HD (2005) Preparation and properties of microencapsulated octadecane with waterborne polyurethane. J Appl Polym Sci 96:1596–1604

Kim BS, Tation TA (2007) Multicomponent nanoparticles via self-assembly with cross-linked block copolymer surfactants. Langmuir 23:2198–2202

Klaypradit W, Huang YW (2008) Fish oil encapsulation with chitosan using ultrasonic atomizer. LWT Food Sci Technol 41:1133–1139

Landfester K (2009) Miniemulsion polymerization and structure of polymer and hybrid nanoparticles. Angew Chem 48:4488–4507

Lee CY, Yu H, Kim ES (2007) Microreactions using nanoliter droplets with oil encapsulation. In: IEEE 20th international conference on micro electro mechanical systems, pp 81–84

Leelajariyakul S, Noguchi H, Kiatkamjornwong S (2008) Surface-modified and micro-encapsulated pigmented inks for ink jet printing on textile fabrics. Prog Org Coat 62:145–161

Liu X, Liu H, Wang S, Zhang L, Cheng H (2006a) Preparation and thermal properties of form stable paraffin phase change materials encapsulation. Energy Convers Manag 47:2515–2522

Liu HY, Cao K, Huang Y, Yao Z, Li BG, Hu GH (2006b) Kinetics and simulation of the imidization of poly(styrene-co-maleic anhydride) with amines. J Appl Polym Sci 100:2744–2749

Luo Y, Gu H (2006) A general strategy for nano-encapsulation via interfacially confined living/controlled radical miniemulsion polymerization. Macromol Rapid Commun 27:21–25

Luo Y, Gu H (2007) Nanoencapsulation via interfacially confined reversible addition fragmentation transfer (RAFT) miniemulsion polymerization. Polymer 48:3262–3272

Luo Y, Zhou X (2004) Nanoencapsulation of a hydrophobic compound by a miniemulsion polymerization process. J Polym Sci A 42:2145–2154

Malardier-Jugroot C, Van de Ven TGM, Whitehead MA (2005) Linear conformation of poly(styrene-alt-maleic anhydride) capable of self-assembly: a result of chain stiffening by internal hydrogen bonds. J Phys Chem B 109:7022–7032

Martin A, Varona S, Navarrete A, Cocero MJ (2010) Encapsulation and co-precipitation process with supercritical fluids: applications with essential oils. Open Chem Eng J 4:31–41

Martinez A, Gonzalez C, Porras M, Gutierez JM (2005) Nanosized latex particles obtained by emulsion polymerization using an amphiphilic block copolymer as surfactant. Colloid Surf A 270–271:67–71

Mazur M (2008) Polypyrrole containers grown on oil microdroplets: encapsulation of fluorescent dyes. Langmuir 24:10414–10420

Mizuno K, Taguchi Y (2005) The effect of the surfactant absorption layer on the growth rate of the polyurethane capsule shell. J Chem Eng Jpn 38:45–48

Mogridge DJ, Phipps JS, Rogan KR, Skuse DR (2002) Pigment dispersion technology for the paper industry. In: Skuse DRS (ed) Specialty chemicals in mineral processing. Royal Society of Chemistry, Cambridge, pp 55–67

Moore E, Pickelman D (1986) Synthesis of styrene/maleimide copolymers and physical properties thereof. Ind Eng Chem Prod Res Dev 25:603–609

Mu B, Shen R, Liu P (2009) Crosslinked polymeric nanocapsules from polymer brushes grafted silica nanoparticles via surface-initiated atom transfer radical polymerization. Colloid Surf B 74:511–515

Muik B, Lendl B, Molina-Diaz A, Ayora MJ (2005) Canada, direct monitoring of lipid oxidation in edible oils by Fourier transform Raman spectroscopy. Chem Phys Lipid 134:173–182

Nguyen D, Zondanos HS, Farrugia JM, Serelis AK, Such CH, Hawkett BS (2008) Pigment encapsulation by emulsion polymerization using macro-RAFT copolymers. Langmuir 24:2140–2150

Peng S, Fuchs A, Wirtz RA (2004) Polymeric phase change composites for thermal energy storage. J Appl Polym Sci 93:1240–1251

Petrovic GM, Stojanovic GS, Radulovic NS (2010) Encapsulation of cinnamon oil in β-cyclodextrin. J Med Plant Res 4:1382–1390

Rong Y, Chen HZ, Wei DC, Sun JZ, Wang M (2004) Microcapsules with compact membrane structure from gelatin and styrene–maleic anhydride copolymer by complex coacervation. Colloid Surf A 242:17–20

Sadeghi-Jorabchi H, Wilson RH, Belton PS, Edwards-Webb JD, Coxon DT (1991) Quantitative analysis of oils and fats by Fourier transform Raman spectroscopy. Spectrochim Acta A 47:1449–1458

Samyn P, Deconinck M, Schoukens G, Stanssens D, Vonck L, Van den Abbeele H (2010) Modification of paper and paperboard surfaces with a nanostructured polymer coating. Prog Org Coat 69:442–454

Samyn P, Deconinck M, Schoukens G, Stanssens D, Vonck L, Van den Abbeele H (2012a) Synthesis and characterization of imidized poly(styrene–maleic anhydride) organic nanoparticles in stable aqueous dispersion. Polym Adv Technol 23:311–325

Samyn P, Schoukens G, Vonck L, Stanssens D, Van den Abbeele H (2012b) Quality of Brazilian vegetable oils evaluated by (modulated) differential scanning calorimetry. J Therm Anal Calorim. doi:10.1007/s10973-011-2132-2

Samyn P, Van Nieuwkerke D, Schoukens G, Vonck L, Stanssens D, Van den Abbeele H (2012c) Quality and statistical quantification of Brazilian vegetable oils using FTIR and Raman spectroscopy. Appl Spectrosc 66:552–565

Sansukcharearnpon A, Wanichwecharungruang S, Leepipatpaiboon N, Kerdcharoen T, Arayachukeat S (2010) High loading fragrance encapsulation based on a polymer-blend: preparation and release behavior. Int J Pharm 31:267–273

Sari A, Alkan C, Karaipekli A, Onal A (2008) Preparation, characterization and thermal properties of styrene–maleic anhydride copolymer (SMA)/fatty acid composites as form stable phase change materials. Energy Convers Manag 49:373–380

Shulkin A, Stöver HDH (2002) Microcapsules from styrene–maleic anhydride copolymers: study of morphology and release behaviour. J Membr Sci 209:433–444

Su JF, Wang LX, Ren L (2006) Fabrication and thermal properties of micro-phase change materials: used melamine formaldehyde resin as shell material. J Appl Polym Sci 101:1522–1528

Su JF, Wang LX, Ren L (2007) Synthesis of polyurethane micro-PCMs containing *n*-octadecane by interfacial polycondensation: influence of styrene–maleic anhydride as surfactant. Colloid Surf A 299:268–275

Szczepanowicz K, Dronka-Gora D, Para G, Warszynski P (2010) Encapsulation of liquid cores by layer-by-layer adsorption of polyelectrolytes. J Microencapsul 27:198–204

Tao M, Hu Z, Zhang Z (2008) Morphology of the poly(styrene-alt-maleic anhydride) micelles obtained by radiation-induced emulsion polymerization using anionic/nonionic mixed surfactants templates. Mater Lett 62:597–599

Tian Y, Zhou W, Yu L, Meng F, Yu K, Ding K, Li M, Wang Z (2007) Self-assembly of monodisperse SiO_2–zinc borate core–shell nanospheres for lubrication. Mater Lett 61:506–510

Torini L, Argillier JF, Zydowicz N (2005) Interfacial polycondensation encapsulation in mini-emulsion. Macromolecules 38:3225–3236

Turchiuli C, Fuchs M, Bohin M, Cuvelier ME, Ordonnaud C, Peyrat-Maillard M (2005) Oil encapsulation by spray drying and fluidised bed agglomeration. Innov Food Sci Emerg Technol 6:29–35

Voncina B, Kreft O, Kokol V, Chen WT (2009) Encapsulation of rosemary oil in ethylcellulose microcapsules. Analysis 1:13–19

Xiao M, Feng B, Gong K (2002) Preparation and performance of shape-stabilized phase change thermal storage materials with high thermal conductivity. Energy Convers Manag 43:103–108

Yow HN, Wu X, Routh AF, Guy RH (2005) Dye diffusion from microcapsules with different shell thickness into mammalian skin. Eur J Pharm Biopharm 72:62–68

Zhang XX, Fan YF, Tao XM, Yick KL (2005) Crystallization and prevention of supercooling of micro-encapsulated *n*-alkanes. J Colloid Interface Sci 281:299–306

Zhong Y, Feng J, Chen S (2005) Dyeing of polyester using micro-encapsulated disperse dyes in the absence of auxiliaries. Color Technol 121:76–80

Zuidam NJ, Nedovic V (2010) Encapsulation technologies for active food ingredients and food processing. Springer, New York